Low-frequency fluctuation amplitude analysis of resting-state fMRI for sickle cell disease patients

Julie Coloigner, Yeun Kim, Adam Bush, Matt Borzage, Vidya Rajagopalan, Natasha Lepore, John Wood

Low-frequency fluctuation amplitude analysis of resting-state fMRI for sickle cell disease patients

Julie Coloigner[a], Yeun Kim[a], Adam Bush[c], Matt Borzage[a,b,c],Vidya Rajagopalan[a], Natasha Lepore[a], and John Wood[c]

[a] CIBORG laboratory, department of Radiology, Children's Hospital, Los Angeles
[b] Department of Neonatology, Childrens Hospital Los Angeles
[c] Division of Cardiology, Childrens Hospital, Los Angeles

ABSTRACT

Sickle cell disease may result in neurological damage and strokes, leading to morbidity and mortality. The inability of conventional magnetic resonance imaging to predict impending stroke underlies the need for other neuroimaging markers risk. In this study, we analyzed neuronal processes at resting state and more particularly how this disease affects the default mode network. The amplitude of low frequency fluctuations was used to reflect areas of spontaneous BOLD signal across brain regions. We compared the activations of sickle cell disease patients to a control group with variance analysis and t-test. Significant differences in different parts among the two groups were observed, especially in the default mode network areas and cortical regions near large cerebral arteries. These findings suggest that sickle cell disease can cause some activation modifications near vessels, and these changes could be used a biomarker of the malady.

Keywords: Functional magnetic resonance imaging, Resting state, Connectivity, Sickle cell disease, amplitude of low-frequency fluctuations

1. INTRODUCTION

Sickle cell disease (SCD) is a chronic blood disorder caused by a mutation in the hemoglobin beta gene that affects millions of people throughout the world, particularly descendents of Sub-Saharan African. Red blood cells lack the flexibility required to flow in the circulatory system, leading to vasoocclusion, ischemia and infarcts. More particularly, SCD can cause neurological damage and strokes, leading to significant mortality and morbidity. Identification of cerebral biomarkers could be useful to predict brain alterations and to diagnose disease states.[1] However, structural magnetic resonance imaging is not sensitive enough to detect biomarkers that may aid in SCD disease stratification. This has highlighted the need to investigate other neuroimaging markers in the brain of SCD patients.[2–4]

Functional Magnetic Resonance Imaging (fMRI) is a non-invasive technique for measuring and mapping the brain activity. Spontaneous low frequency fluctuations of Blood Oxygenation Level-Dependent (BOLD) signal have been observed during rest and can be identified with baseline spontaneous activity in the brain. The default mode network (DMN) which consists of the precuneus, posterior cingulate cortex, medial prefrontal cortex and lateral parietal cortex[5] is of particular interest. Indeed, in a growing number of studies, the activity within the DMN is analyzed to understand how spontaneous synchronized activity of neuronal populations is altered in diseases such as depression, Alzeihmer's diseases, schizophrenia or epilepsy.[6,7]

In this paper, we analyze the resting state functional magnetic resonance signal, whose low-frequency fluctuations are considered to reflect spontaneous synchronized activity of neuronal populations. The Amplitude of Low Frequency Fluctuations (ALFF)[8] is used to determine areas of spontaneous BOLD signal across brain regions. Given the cognitive deficits and abnormal blood flow in SCD patients, we hypothesize that significant alterations in DMN activation patterns exist between patients with SCD and control subjects. These abnormalities may be a trait marker and could be helpful for the future diagnosis of SCD stages.

2. MATERIAL AND METHODS

2.1 Dataset

This study was approved by institutional review board (CCI#1100083) and conducted in the Children's Hospital Los Angeles (CHLA) between January 2012 and May 2015. Written informed consent was obtained from all subjects. Since 70% of SCD patients develop stroke by 20 years of age, we restricted our population to adolescents and young adults without strokes. 20 SCD patients (age=23 $\pm$ 8) and 17 control subjects (age=21 $\pm$ 1) were included in this analysis. Exclusion criteria included pregnancy, previous stroke, acute chest or pain crisis hospitalization within one month. The patients were group-matched in terms of sex and education. All participants underwent a battery of tests: structural and functional imaging and neurophysiological tests.

MRI data were acquired on a 3T Philips Achieva at CHLA. A 3D T1-weighted image was acquired covering the whole brain (160 sagittal slices) with TR = 8.20 s, TE = 3.77 ms, flip angle = 8, in-plane resolution = 256 $\times$ 256, FOV = 256 mm $\times$ 224 mm and thickness/gap =1.0/0 mm). During resting-state fMRI scanning, subjects were instructed to close their eyes and keep still as much as possible, and not to think of anything systematically or fall asleep. The functional images were acquired with the following parameters: TR = 2000 ms, TE = 50 ms, flip angle = 90, in-plane resolution = 96 $\times$ 96, FOV = 220 mm $\times$ 220 mm, 26 axial slices, thickness/gap= 5/0 mm. A total of the 240 volumes were collected in 8 minutes.

2.2 Preprocessing steps

The resting-state fMRI data were preprocessed with the FMRIB Software Library (FSL), using standard spatial preprocessing methods. The first 5 volumes from each subject were discarded to allow the signal to reach equilibrium and to allow the participant to adapt to the scanning noise. The remaining 235 volumes were corrected for the acquisition time delay between slices. Rigid realignment was then performed to remove physiological motion such as high-frequency respiratory and cardiac noise, with FSLs MCFLIRT. A motion index, DVARS, which represents the change in BOLD signal from volume to volume, was then computed. This measure was calculated as the root mean squared value of the differentiated time series (by backwards differences). Some volumes were excluded because of excessive DVARS.

Then, a two-step coregistration method was used to transform the fMRI data into the Montreal Neurological Institute (MNI) template space. First, the mean fMRI image was coregistered (6 parameters) with the structural image; then these structural images were linearly transformed to the Montreal Neurological Institute (MNI) template space, using the FLIRT and FNIRT algorithms of FSL. The generated parameters for these two coregistration steps were then concatenated and used for the normalization of each fMRI volume. Finally, the registered fMRI volumes were normalized and smoothed with a Gaussian kernel of 8mm $\times$ 8mm $\times$ 8mm full-width at half maximum (FWHM).

After fMRI preprocessing, in order to remove residual motion, the parameters estimated by FSL's MCFLIRT, as well as their derivatives were used as regressors, computed by backwards differences (12 regressors). Moreover, the physiological noise was also reduced using other nuisance regressors which were calculated by the CompCor[9] method as implemented in Nilearn (http://nilearn.github.io/). These 5 regressors correspond to the principal components from noisy regions-of-non-interest, such as white matter, cerebral spinal fluid, and out-of brain. Then, the fMRI data were temporally band-pass filtered ($0.009 < f < 0.08$ Hz) to reduce the very low-frequency drift and high-frequency respiratory and cardiac noise.

2.3 ALFF analysis

The ALFF analysis[10] was performed using FSL functions. The power spectrum was obtained after the time series for each voxel were transformed to the frequency domain with a Fast Fourier Transform (FFT). Since the power of a given frequency is proportional to the square of the amplitude of this frequency component of the original time series in the time domain, the square root was calculated at each frequency of the power spectrum. The averaged square root was obtained across $0.009 - 0.08$ Hz for each voxel. This averaged square root was taken as the ALFF. To reduce global effects of variability across the participants, the ALFF value at each voxel location was divided by the global mean ALFF value. The individual map was transformed to a Z score (i.e., we subtracted the global mean value, and then divided by the standard deviation) instead of being simply divided by the global mean.

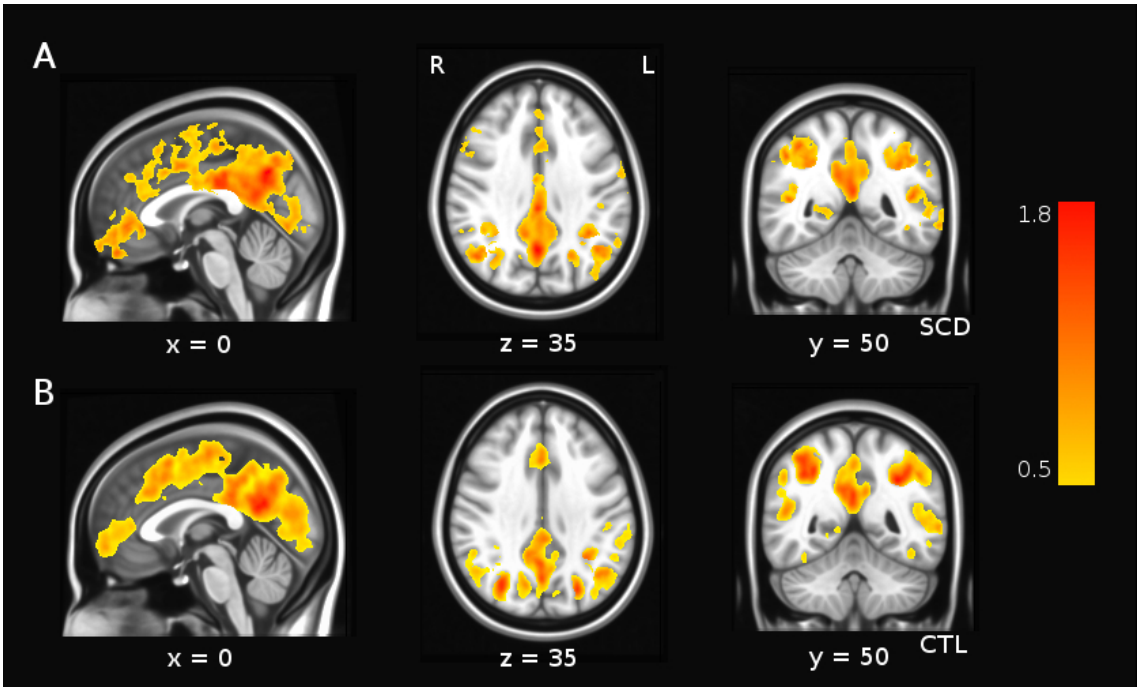

Figure 1. Representative one-sample t-test results of ALFF maps ($P < 0.05$, AlphaSim corrected) in groups of SCD (A) and control (B) subjects. Color scale indicates t values. Thresholds were set at a corrected $p < 0.05$, determined by Monte Carlo simulation. The planes are $X = 0$, $Y = 50$ and $Z = 35$ for the sagittal, coronal and axial views, repectively, in the Montreal Neurological Instititute (MNI) template.

2.4 Statistical Analysis

2.4.1 Within-group ALFF analysis

To explore the within-group whole-brain ALFF patterns, one-sample t-tests were performed on the individual ALFF maps in a voxelwise manner for the two groups: SCD and control. A gray matter mask of the MNI template was used. The corrected threshold was determined using the AlphaSim program[11] with a p-value threshold set at $P < 0.05$ and a cluster size > 1.91 cm^3.

2.4.2 Between-group ALFF analysis

To investigate the variability of the activation, one-way analysis of variance (ANOVA) was performed to determine the ALFF differences among the two groups at each voxel (within a gray matter mask). The statistical map was corrected again using the AlphaSim program, with the threshold set at $P < 0.05$ and a cluster size larger than 1.91 cm^3. After identifying all significant clusters, we made a mask including these regions. A post hoc t-test was then performed to compare the Z-maps of the activations between the patient and control groups, restricting the analysis within this mask.

3. RESULTS

As illustrated in the Figure 1, within each group, significant higher ALFF was found in several brain regions, such as medial prefrontal cortex (mPFC), posterior cingulate cortex (PCC), precuneus and posterior frontal cortex.

The one-way ANOVA revealed 8 clusters with significant differences across the SCD and control groups, including medial orbitofrontal cortex (MOFC), anterior cingulate cortex (ACC), Brodmann Area 8 (BA 8), posterior region of middle cingulate cortex, posterior cingulate cortex (PCC), anterior lobe of cerebellum, posterior lobe of cerebellum and parietooccipital sulcus, as shown in table 1 and figure 2. Table 1 illustrates the results of the t-test for these 8 regions. Compared with the control subjects, the SCD patients showed a significant

Cerebral region	MNI coordinates	Cluster volume (mm^3)	F-value	t-value
(1) Decreased regions				
Medial orbitofrontal cortex	[-3,-31,-8]	28950	11.94	-3.76
Posterior region of middle cingulate cortex	[-2,26,36]	1542	6.81	-1.82
Posterior cingulate cortex	[5,44,44]	1467	6.72	-2.64
(2) Increased regions				
Anterior cingulate cortex	[-13,-52,-2]	1542	5.11	3.09
Brodmann Area 8	[-2,-19,43]	7.03	6.46	2.95
Anterior lobe of cerebellum	[3,60,-12]	1011	9.58	2.99
Posterior lobe of cerebellum	[6,78,-27]	1317	8.30	1.90
Parietooccipital sulcus	[20,74,35]	1304	5.53	3.19

Table 1. List of brain areas with significant differences in ALFF during the resting state between the SCD and control groups. A positive sign in the peak t-value represents an increase, while a negative one represents a decrease in SCD group. A corrected threshold of $p < 0.05$ determined by Monte Carlo simulation was taken as meaning that there was a significant difference between groups for either t-test and ANOVA test.

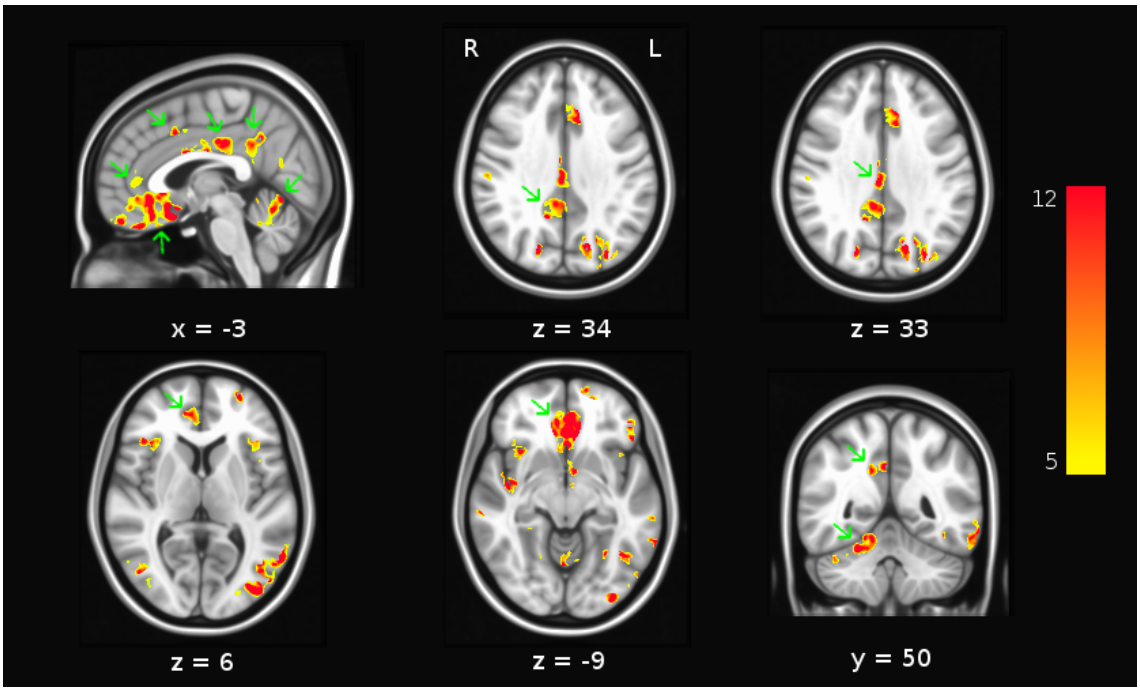

Figure 2. Representative one-way ANOVA results of ALFF maps ($P < 0.05$, AlphaSim corrected) between SCD and control groups. On the the sagittal view (higher, left), five clusters are displayed by arrows (counter-clockwise): medial orbitofrontal cortex, anterior cingulate cortex, Brodmann Area 8 (BA 8), posterior region of cingulate cortex, posterior cingulate cortex and anterior lobe of cerebellum. In the axial views, the regions indicated by arrows are as follows: posterior cingulate cortex (Z=34), posterior region of middle cingulate cortex (Z=33), anterior cingulate cortex (Z=6), medial orbitofrontal cortex (Z=-9). In the coronal view, the anterior lobe of cerebellum is signed by an arrow.

decrease in ALFF in PCC, posterior region of cingulate cortex and MOFC. In addition, an increased activity in ACC, BA 8, cerebellum and parietooccipital sulcus was found in the sickle cell disease group.

4. DISCUSSION

Using the ALFF metric of resting state fMRI, several neuronal activity changes were detected in specific brain regions in SCD patients versus control subjects. These neuronal abnormalities were found in 8 areas in the SCD group. This may be due to a variety of factors, including for example fear extinction, tissue damage from strokes, and vasculature differences that are not apparent on MR imaging.

The analysis of ALFF indicated that patients with sickle cell disease showed differences in activity within regions of the DMN. First, we observed that resting-state functional connectivity of the ACC was increased in patients with SCD when compared to control subjects. Previous studies have found a strong association between ACC and the emotional response to pain.[12] Buchel et. al.[13] found a positive correlation between fMRI signal intensity and pain intensity. Since most SCD patients suffer from episodic or chronic pain, it seems plausible that their ACC will show abnormally increased activity.

Secondly, we observed a decreased activity in the posterior components of the DMN, the PCC and precuneus, which are thought to act as intrinsic mediatory nodes of this network.[14] Regional differences in cortical thickness from SCD patients were also located on the posterior medial surfaces, the so-called "watershed" areas between the perfusion territories of the anterior cerebral artery (ACA) and the posterior cerebral artery (PCA).[15] The precuneus and the posterior cingulate are vulnerable to acute anemia and, thus, may be susceptible to abnormal development.

The orbitofrontal cortex covers the ventral surface of the primate prefrontal cortex. Several animal studies as well as human neuroimaging studies have reported that the medial orbitofrontal cortex (mOFC) and the ventromedial prefrontal cortex (vmPFC) are associated with fear extinction.[16–21] We found these areas to have lower ALFF values in the SCD patients than in the control group. We attribute this phenomenon to the heightened level of fear and anxiety of the control group due to their unfamiliarity to hospital exams and environment. Since the SCD patients are more used to hospital setting and exams, the lower ALFF value may reflect these differences.

Lastly, we observed four regions with abnormal activity in the SCD group: Brodmann Area 8, anterior lobe of cerebellum, posterior lobe of cerebellum and parietooccipital sulcus. In fMRI studies, BOLD signals are often affected by vascular activities, causing the signals to fluctuate. Thus, the ALFF values of these four regions may be affected by vasculature, since they are located near large cerebral arteries such as the ACA, the superior cerebellar artery, the anterior inferior cerebellar artery and the parieto-occipital branch of posterior cerebral artery, respectively.

5. CONCLUSION

In this paper, we studied the brain functional activation, using the ALFF analysis. Our comparison among the SCD and control groups confirmed our hypothesis about the difference in resting state activity for SCD patients, and revealed a difference in DMN and cortical regions near large cerebral arteries. The next step will consist in taking into account different measures in the study, such as the localization of the damage, venous vasculature and physiological parameters.

REFERENCES

[1] Elias, E., Liao, J., Jara, H., Watanabe, M., Nadgir, R., Sakai, Y., Erbay, K., Saito, N., Ozonoff, A., Steinberg, M., and Sakai, O., "Quantitative mri analysis of craniofacial bone marrow in patients with sickle cell disease," *J. Neuroradiol.* **34**(3), 622–7 (2013).

[2] Steen, R. G., Emudianugh, T., Hunte, M., Glass, J., Wu, S., Xiong, X., and Reddick, W., "Brain volume in pediatric patients with sickle cell disease: evidence of volumic growth delay?," *AJNR Am J Neuroradiol.* **26**(3), 455–62 (2005).

[3] Kirk, G. R., Haynes, M. R., Palasis, S., Brown, C., Burns, T. G., McCormick, M., and Jones, R. A., "Regionally specific cortical thinning in children with sickle cell disease," *Cerebral Cortex* **19**, 1549–1556 (2009).

[4] Balci, A., Karazincir, S., Beyoglu, Y., Cingiz, C., Davran, R., Gali, E., Okuyucu, E., and Egilmez, E., "Quantitative brain diffusion-tensor mri findings in patients with sickle cell disease," *American Journal of Roentgenology* **198**(5), 1167–74 (2012).

[5] Raichle, M., MacLeod, A., Snyder, A., Powers, W., Gusnard, D., and Shulman, G., "A default mode of brain function," *Proc Natl Acad Sci* **98**(2) (2001).

[6] Fox, M. and Greicius, M., "Clinical applications of resting state functional connectivity," *Front Syst Neuroscience* , 4–19 (2010).

[7] Qi, Z., Wu, X., Wang, Z., Zhang, N., Dong, H., Yao, L., and Li, K., "Impairment and compensation coexist in amnestic mci default mode network," *Neuroimage* **50**, 48–55 (2010).

[8] Zou, Q.-H., Zhu, C.-Z., Yang, Y., Zuo, X.-N., Long, X.-Y., Cao, Q.-J., Wang, Y.-F., and Zang, Y.-F., "An improved approach to detection of amplitude of low-frequency fluctuation (alff) for resting state fmri: Fractional alff," *J. of Neuroscience Methods* **172**, 137–141 (2008).

[9] Behzadi, Y., Restom, K., Liau, J., and T.Liu, "A component based noise correction method (compcor) for bold and perfusion based fmri," *Neuroimage* **375(1)**, 90–101 (2007).

[10] Qi, R., Zhang, L., Wu, S., Zhong, J., Ni, L., Zhang, Z., Li, K., Jia, Q., Wu, X., Liu, Y., and Lu, G., "Altered resting-state brain activity at functional mr imaging during the progression of hepatic encephalopathy," *Radiology* **264** (2012).

[11] Ledberg, A., Akerman, S., and Roland, P., "Estimation of the probabilities of 3D clusters in functional brain images," *Neuroimage* **8**, 113–128 (1998).

[12] Baliki, M. N., Mansour, A. R., Baria, A. T., and Apkarian, A. V., "Functional reorganization of the default mode network across chronic pain conditions," *Plos One* (2014).

[13] Bchel, C., Bornhvd, K., Quante, M., Glauche, V., Bromm, B., and Weiller, C., "Dissociable neural responses related to pain intensity, stimulus intensity, and stimulus awareness within the anterior cingulate cortex: a parametric single-trial laser functional magnetic resonance imaging study," *The Journal of Neuroscience* **22**, 970–976 (2002).

[14] Cavanna, A. and Trimble, M., "The precuneus: a review of its functional anatomy and behavioural correlates," *Brain* **129**, 564–83 (2006).

[15] Kirk, G., Haynes, M., Palasis, S., Brown, C., Burns, T., McCormick, M., and Jones, R., "Regionally specific cortical thinning in children with sickle cell disease.," *Cereb Cortex* **19**, 1549–56 (2009).

[16] Milad, M., Rauch, S., Pitman, R., and Quirk, G., "Fear extinction in rats: implications for human brain imaging and anxiety disorders," *Biol. Psychol.* **73**, 61–71 (2006).

[17] Barad, M., "Fear extinction in rodents: basic insight to clinical promise," *Curr. Opin. Neurobiol* **15**, 710715 (2005).

[18] Sotres-Bayon, F., Cain, C., and Ledoux, J., "Brain mechanisms of fear extinction: historical perspectives on the contribution of prefrontal cortex," *Biol. Psychiatry* **60**, 329336 (2006).

[19] Rauch, S., Shin, L., and Phelps, E., "Neurocircuitry models of posttraumatic stress disorder and extinction: Human neuroimaging researchpast, present and future," *Biol. Psychiatry* **60**, 376382 (2006).

[20] Quirk, G., Garcia, R., and Gonzalez-Lima, F., "Prefrontal mechanisms in extinction of conditioned fear," *Biol. Psychiatry* **60**, 337343 (2006).

[21] Davis, M., Myers, K., Chhatwal, J., and Ressler, K., "Pharmacological treatments that facilitate extinction of fear: relevance to psychotherapy," *NeuroRx* **3**, 8296 (2006).